Supramolecular Ordering of PTCDA Molecules: The Key Role of Dispersion Forces in an Unusual Transition from Physisorbed into Chemisorbed State

Szymon Godlewski,[†,*] Antoni Tekiel,[†,‡] Witold Piskorz,[§,*] Filip Zasada,[§] Jakub S. Prauzner-Bechcicki,[†] Zbigniew Sojka,[§] and Marek Szymonski[†]

[†]Faculty of Physics, Astronomy and Applied Computer Science, Jagiellonian University, Reymonta 4, 30-059 Krakow, Poland, [‡]Department of Physics, McGill University, 3600 University Street, Montreal, Quebec H3A 2T8, Canada, and [§]Faculty of Chemistry, Jagiellonian University, Ingardena 3, 30-060 Krakow, Poland

ABSTRACT

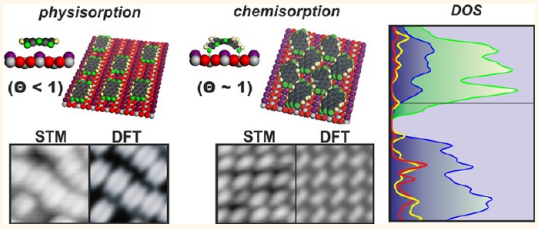

Adsorption and self-assembly of large π-conjugated 3,4,9,10-perylene tetracarboxylic dianhydride (PTCDA) molecules on rutile TiO_2(110) surface have been investigated using a combination of high-resolution scanning tunneling microscopy (STM), low-energy electron diffraction, and density functional theory calculations with inclusion of Grimme treatment of the dispersion forces (DFT-D). Evolution of the STM images as a function of PTCDA coverage is caused by transition of the adsorption mode from physisorbed single adspecies and meandering stripes into spontaneously ordered chemisorbed molecular assemblies. This change in the adsorption fashion is accompanied by significant bending of the intrinsically flat, yet elastic, PTCDA molecule, which allows for strong electronic coupling of the dye adspecies with the TiO_2 substrate. Extensive DFT-D modeling has revealed that adsorption is controlled by interfacial and intermolecular dispersion forces playing a dominant role in the adsorption of single PTCDA species, their self-organization into the meandering stripes, and at the monolayer coverage acting collectively to surmount the chemisorption energy barrier associated with the molecule bending. Analysis of the resulting density of states has revealed that alignment of the energy levels and strong electronic coupling at the PTCDA/TiO_2 interface are beneficial for dye sensitization purposes.

KEYWORDS: supramolecular ordering · titanium dioxide · TiO_2 · PTCDA · dye sensitization · photovoltaics · STM · DFT-D · van der Waals · semi-empirical dispersion · adsorption · DOS · surface functionalization

Supramolecular self-assembly of organic molecules on surfaces plays an important role in nanofabrication. It can control formation and properties of nanostructures, leading to a wide range of applications in photovoltaics, (opto)electronics, gas sensing, (photo)catalysis, and in medicine.[1−7] Among many types of substrates used for surface-supported supramolecular assembly, metal oxides appear very attractive due to their tunable electronic structure and versatile chemical properties. TiO_2, the most frequently studied material among transition metal oxides, plays a dominant role in model studies and practical applications, especially in conjunction with organic dye sensitization for photovoltaic devices.[8−11] One of the key challenges for molecular nanofabrication is an effective control of the intermolecular interactions and the binding between the deposited species and the substrate surface. In our work, we have chosen PTCDA molecules,[12−19] which are extensively studied prototypes of large π-conjugated molecules and are widely used in optoelectronic and photovoltaic devices, to demonstrate the central role of collective intermolecular dispersion forces in controlling the supramolecular ordering of admolecules on the TiO_2 surface.

Although the density functional theory (DFT) methods have been widely used in analysis of surface-supported molecular systems,[20−28] still little is known about the nature of the binding of large aromatic planar molecules on metal oxide surfaces. Most studies, so far, have been based on standard DFT calculations,[29−31] without an explicit account for sizable van der Waals interactions that can actually play a significant role due to the presence of large and highly polarizable polyaromatic rings.[32,33] The size limitation makes the semi-empirical Grimme extension of the standard DFT method (denoted as DFT-D) an attractive and computationally cost-effective way of incorporating dispersion interactions.[32,34−41] In recent years, this approach has demonstrated its ability to provide reliable modeling of molecular

* Address correspondence to szymon.godlewski@uj.edu.pl, wpiskorz@chemia.uj.edu.pl.

Received for review February 28, 2012 and accepted September 12, 2012.

Published online September 12, 2012
10.1021/nn303546m

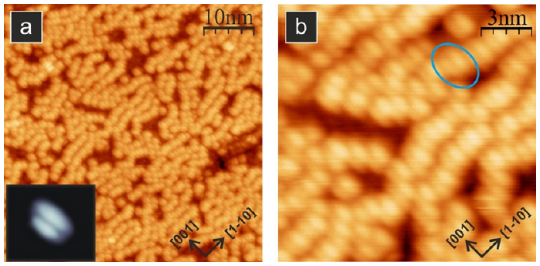

Figure 1. (a) Empty state STM images of meandering molecular stripes together with an isolated molecule (inset). (b) Magnification of the left image reveals the characteristic two-lobe appearance and the orientation of PTCDA with the longer axis parallel to the [001] direction (blue ellipse indicates a single molecule). Both STM images were acquired with the bias voltage of +2.0 V and the tunneling current of 2 pA.

geometries and better description of the molecule–metal substrate binding.[33,42,43] Until now, in the case of metal oxide substrates, the DFT-D methods have been used for modeling small inorganic systems[44,45] and alkyl chains only.[46] In particular, almost no attempt has been made yet to analyze adsorption of large aromatic systems.

In the present work, we examined the role of the interfacial and intermolecular dispersion forces in nanofabrication of large π-conjugated systems on metal oxide surfaces by thorough experimental and theoretical investigations of PTCDA molecules deposited on the TiO_2(110) surface. The PTCDA/TiO_2 system was characterized by high-resolution low-temperature scanning tunneling microscopy (STM) and low-energy electron diffraction (LEED), complemented by DFT-D modeling, including the Tersoff–Hamann[47] and more advanced Bardeen[48] simulations of the STM images.

RESULTS AND DISCUSSION

Low Coverage Limit: Physisorbed PTCDA Molecules. PTCDA molecules were thermally deposited on the TiO_2(110) substrate at room temperature under ultrahigh vacuum conditions. At low coverage, the molecules adsorb flat as single entities with their longer molecular axis oriented along the [001] direction of the titania substrate, that is, along the surface bridging oxygen rows. The characteristic two-lobe appearance in the STM images (two dominant lobes of the LUMO orbital spread parallel to the longer molecular axis; see inset in Figure 1a) was rationalized through the DFT-D calculations as a physisorption state that essentially only slightly deforms the intrinsically flat geometry of PTCDA. By increasing the coverage to a submonolayer range, the enhanced intermolecular interactions led to formation of meandering molecular stripes running essentially across surface oxygen rows, as shown by STM images in Figure 1 (both panels). The detailed analysis of the STM image (recorded with larger scale in Figure 1b) revealed that the characteristic two-lobe

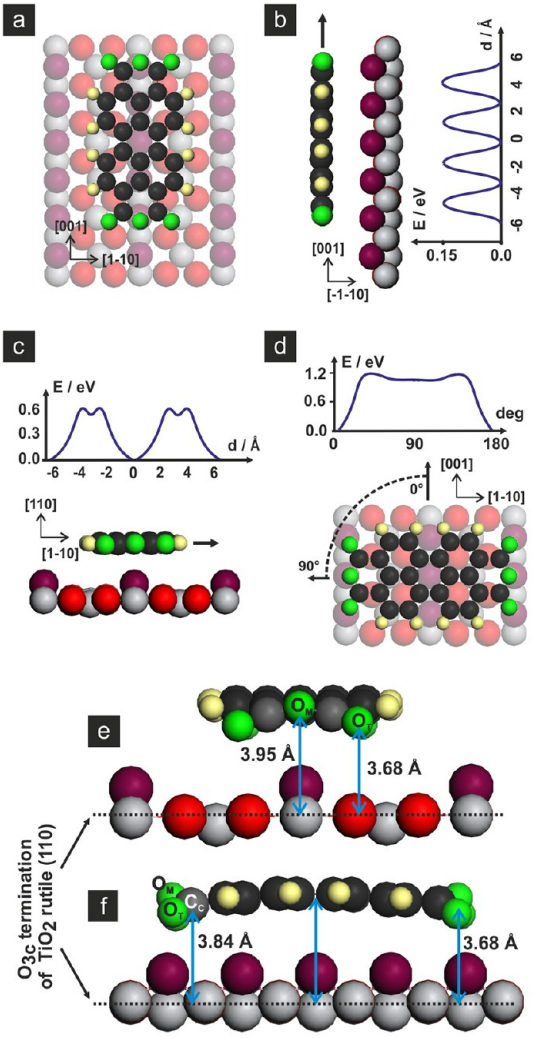

Figure 2. Different views of the most stable adsorption geometry of an isolated PTCDA molecule on the TiO_2-(110) surface. Stable adsorption geometry (a), dependence of the adsorption energy (with respect to the most stable geometry) on the lateral displacement along (b) and across (c) the reconstruction rows. Dependence of the interaction energy on the rotation of the molecule around the axis normal to the surface (d), and deformation of the adsorbed molecule in the most stable geometry (e,f).

appearance of the PTCDA molecules persists, indicating that in this state the admolecules are still bound to the surface by a similar mechanism as in the case of the isolated molecules.

Preliminary GGA-DFT calculations for the flat-lying PTCDA molecule on the TiO_2(110) surface revealed the presence of weak (about 0.15 eV per molecule) attractive molecule–substrate interactions only, which do not favor any specific orientation of the molecules, in apparent contradiction to the STM observations. Thus, to correctly describe the adsorption, we used the DFT-D scheme to investigate the potential energy surface (PES) of the PTCDA/TiO_2 system in more detail. The starting point was the fully optimized PTCDA molecule located directly above the protruding oxygen rows, as

shown in Figure 2a. The TiO_2 surface was then scanned by dragging the PTCDA molecule along the [001] (Figure 2b) and [1−10] (Figure 2c) directions and by rotating it around the [110] axis (Figure 2d). As presented in the corresponding energetic profiles, the movement along the [001] direction was accompanied by a periodic variation of the potential energy with the amplitude of 0.15 eV (Figure 2b). The movement across the protruding oxygen rows exhibited two energetic minima: a shallow one of 0.1 eV and a deeper one of 0.6 eV (Figure 2c), whereas the rotation around the [110] axis was accompanied by the highest energetic barrier of 1.2 eV (Figure 2d). Thus in the DFT-D scheme, the most stable position of the PTCDA molecule corresponds to the orientation with its main axis parallel to the [001] direction, in a perfect agreement with the STM experiments (see Figure 1). Inspection of Figure 2 reveals that the surface−molecule interactions give rise to only a slight deformation of the polyaromatic backbone with the terminal oxygen atoms (O_T) of the anhydride groups (placed 3.68 Å above the reference plane defined by the surface trigonal oxygen ions) pointing toward the titanium atoms, and the middle part of the carbon ring displaced away from this plane by 4.02 Å. Analysis of the geometry of the anhydride groups indicated that attraction of the O_T atoms toward the surface titanium ions is balanced by repulsion between the middle O_M atoms and bridging oxygens of the TiO_2 substrate (Figure 2f). The elucidated structure of the PTCDA species exhibited the binding energy of 1.76 eV with a dominant contribution of the interfacial dispersion interactions (1.45 eV), which is tantamount with a virtually van der Waals character of the PTCDA−TiO_2 interactions. The appreciable distortion of the inherently planar PTCDA molecule upon adsorption, revealed for the first time on oxide surfaces, is analogous to the morphologies that previously have been observed for PTCDA on the metallic Ag(111) substrate.[49]

The obtained results indicate an excellent agreement between the calculated and experimentally observed geometries of the PTCDA/TiO_2(110) system, confirming the adequacy of the applied DFT-D scheme. Thorough analysis of the results (see Supporting Information Table S1) showed that screening effects are negligible, revealing a dominant role of the dispersion interactions in the adsorption of large polyaromatic molecules on titanium dioxide.

The corresponding Tersoff−Hamann simulations performed for the adsorbed PTCDA in the most stable position (Figure 2a) remain in good agreement with the above conclusions. The simulated image appears as a two-lobe feature characteristic of an essentially intact molecule in the physisorbed state (Figure 3b,c, simulated with different values of Gaussian blurring to include tip broadening effects), which is very similar to that observed in the experimental images recorded for

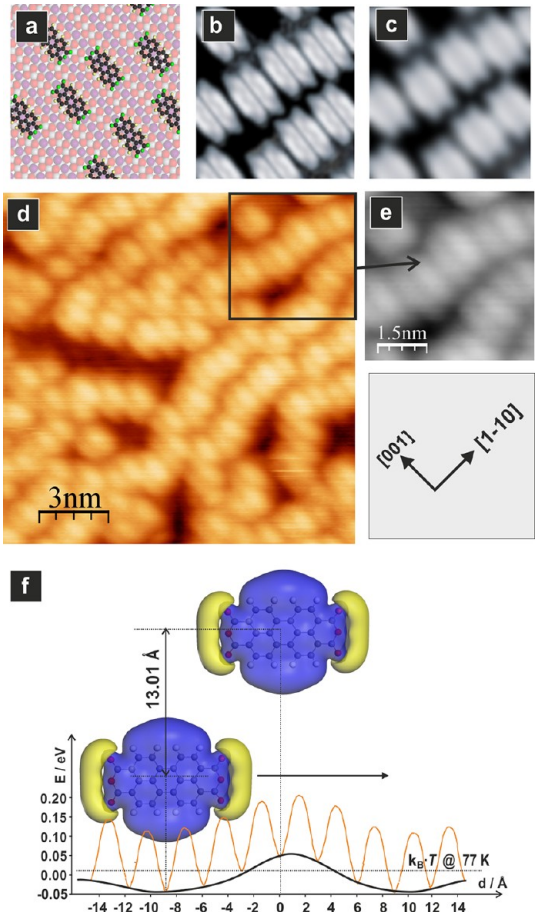

Figure 3. Adsorption of PTCDA molecules on TiO_2 at submonolayer coverage. (a) Schematic model of meandering molecular lines. (b,c) Tersoff−Hamann simulated STM images with varied Gaussian blurring to include tip broadening of the images. (d,e) Empty state STM images of meandering molecular stripes. (f) Overall potential (undulated orange line) produced by interaction potential between two PTCDA molecules while passing by each other (thick black line), superimposed on the PTCDA-surface interaction potential; yellow/violet contour visualizes the negative/positive electrostatic potential isosurfaces. All STM images were acquired with the bias voltage of +2.0 V and the tunneling current of 2 pA.

the submonolayer coverages (Figure 3d,e). As a result, it shows that the PTCDA admolecules in both the isolated and the submonolayer case are essentially physisorbed on the TiO_2 surface. Thus, formation of the meandering molecular stripes can be attributed to the collective action of the intermolecular dispersive forces, which are further enhanced by mutual interactions between the sizable permanent quadrupole moments of the adjacent PTCDA molecules. The development of the stripes was rationalized by a series of DFT-D calculations for a fixed PTCDA molecule being passed (without geometry relaxation) by another one at the distance equal to that observed on the TiO_2 surface in STM scans (the neighboring molecules are located on every second protruding oxygen row, *i.e.*, 13.01 Å apart). Although such a simplified approach does not include the substrate explicitly, it allows for a

quick and rough estimation of the intermolecular interaction potential at low computational costs. The results are shown in Figure 3f, where the solid black line indicates the estimated intermolecular potential that is superimposed on the periodic interaction potential between the PTCDA molecule and the TiO_2 surface (Figure 3f; as a benchmark, the average thermal energy, *kT*, at 77 K is also indicated). The resultant overall potential (marked with the orange line in Figure 3f) exhibits a regular pattern of the preferred energetic positions of the PTCDA molecules relative to the adjacent one. Consequently, alignment of neighboring admolecules along specific directions, such as [2−20], [2−2±1], and [2−2±2], is preferred. This model based on intermolecular dispersion forces rationalizes the self-assembly of the meandering PTCDA stripes on the TiO_2 surface at medium submonolayer coverages (Figures 1 and 3) in a straightforward way. It is worth noting that exclusion of the dispersion forces (apart from the seizing interfacial stabilization) smears out the intermolecular interaction potential by reducing it from 0.11 to 0.01 eV, which would substantially attenuate the driving force of self-organization into the observed pattern.

Since the interactions between the adjacent PTCDA molecules are rather weak, the meandering stripes are metastable and, upon thermal annealing, can readily be transformed into more robust supramolecular assemblies.

Development of Monolayer Coverage: Chemisorption Forced by Dispersion Interactions. The impact of the dispersion forces was even more pronounced once a full PTCDA monolayer was deposited. Indeed, upon increasing the number of the neighboring molecules, an entirely new ordered PTCDA phase was formed. The LEED measurements (see Supporting Information, Figure S1) showed that the new molecular layer exhibits a six-fold commensurability along the protruding oxygen rows ([001] direction), and a two-fold periodicity across the rows ([1−10] direction). Close examination by low-temperature STM indicated that the PTCDA molecules form the structure of a brick-wall-like appearance with a $c(6 \times 2)$ symmetry in the STM images (Figure 4, both panels). On the basis of those observations, we can deduce that this new structure is so densely packed that the accommodation of the flat-lying molecules as nearest neighbors is no longer possible, taking into account sole geometrical constraints of the flat intact molecule only. Noting the large size of the PTCDA molecule and its possible deformation upon adsorption, we have analyzed its flexibility along vertical (long), horizontal (short), and diagonal axes (see Supporting Information, Figure S7). Calculations revealed that the most likely direction of the PTCDA deformation is along the diagonal axis with the elastic modulus of 3.1 eV/Å^2. Deformations along the vertical and horizontal axes are substantially smaller due to considerably higher

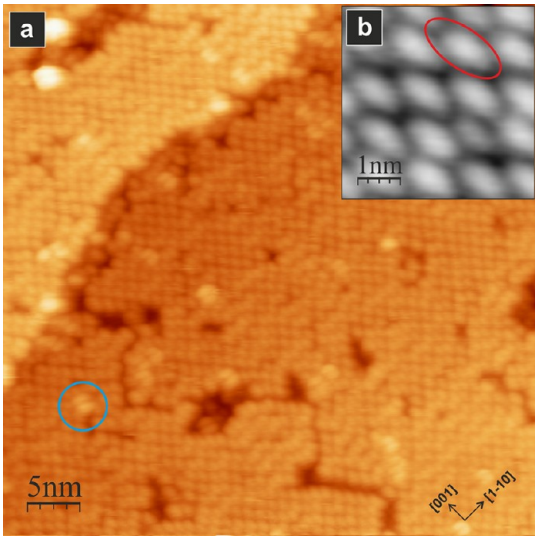

Figure 4. STM image of a densely packed molecular structure (approximately 1 ML). (a) Closed layer (blue circle indicates a single molecule adsorbed on top of the first monolayer). (b) Magnification of the monolayer structure (red ellipse indicates a single molecule). The STM image was acquired with the bias voltage of +2.0 V and the tunneling current of 2 pA.

rigidity of the molecule in these directions (5.4 and 21.7 eV/Å^2, respectively). Such diagonal deformation might rationalize the observed enhanced packing and is beneficial for formation of the strong bonds with the surface that will be discussed in the following paragraph.

Furthermore, there is a striking difference between the typical two-lobe STM contrast of the physisorbed PTCDA molecules observed at the submonolayer coverage and the PTCDA appearance within the dense monolayer, where each molecule was recorded as a single-lobe feature only (a red ellipse in Figure 4b indicates a PTCDA molecule discriminated in the monolayer). It is worth noting that in the same picture there are some individual molecules adsorbed on top of the first monolayer, and they consequently exhibit the two-lobe appearance typical for the physisorbed state (see blue circle in Figure 4a). These observations indicate clearly that there is a significant difference in the electronic structure of the PTCDA molecules adsorbed within the first monolayer, which are recorded as the single-lobe features, and the physisorbed PTCDA molecules (single molecules, meandering stripes, and single molecules adsorbed on top of the first layer) exhibiting the two-lobe STM appearance. To elucidate the structure of the PTCDA molecules in the first monolayer in more detail, a corroborative DFT-D modeling was next performed.

Figure 5a,b shows the most stable monolayer model that adequately reproduces both the surface packing density and the symmetry of the molecular species deduced from the LEED and STM measurements (for analysis of other examined models, see Supporting

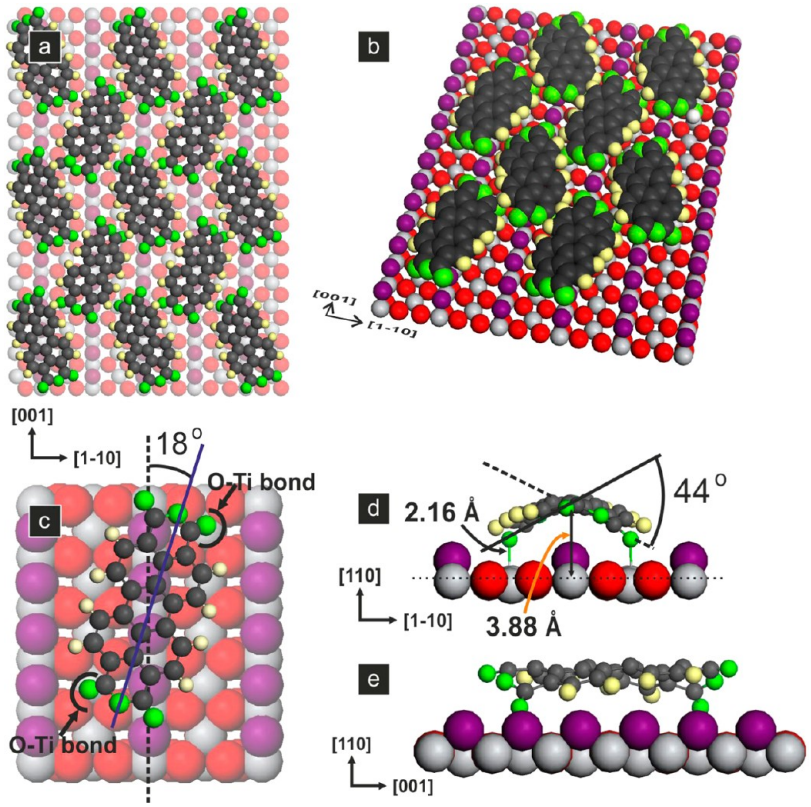

Figure 5. Optimized geometry of the (6 × 2) closed monolayer. Molecules are bent due to dispersion interactions resulting in a quasi-herringbone structure: (a) top view, (b) perspective view, (c−e) single molecule position extracted from the monolayer.

Information, Figure S2 and Table S2). In the optimized geometry exhibiting symmetry compatible with the one observed experimentally, the PTCDA molecules are arched over the protruding surface oxygen rows, with one of their diagonals located on top of the oxygen row (Figure 5c). As a result, two strong covalent bonds between the terminal (O_T) oxygen atoms of PTCDA and the surface titanium atoms can be formed, giving rise to robust coupling between PTCDA and TiO_2 moieties that is beneficial for efficient photosensitization. The two oxygen atoms involved in the bonds creation come from two opposite anhydride terminal groups and are located along one of the molecule diagonals (Figure 5c). In this geometry, the twisting angle between the anhydride groups is 44° and the O_T-Ti_{surf} distance is equal to 2.16 Å. The average distance between the middle aromatic ring of the PTCDA molecule and the surface O_{3c} atoms is 3.88 Å (Figure 5d). The characteristic feature of this configuration is that diagonal hydrogen atoms point toward the surface, in contrast to another slightly less stable configuration (by 0.11 eV) with hydrogen atoms pointing outward from the surface. However, such small difference in geometry has dramatic consequences on the appearance of the STM images (see below).

The described geometrical parameters show dramatic deformation of the PTCDA molecules upon adsorption. Reaching this conformation requires either tight packing leading to increased intermolecular dispersive interactions (approximately 2.22 eV per molecule) or thermal annealing of the meandering stripes to 100 °C. Both of these factors assist in the formation of quite strong chemical bonds (1.08 eV) between the arched PTCDA molecules and the TiO_2 surface. Although the deformation of the intrinsically flat PTCDA molecule implies an energy rise of 0.52 eV, the overall adsorption energy of 2.79 eV per molecule is still sizable. As a result, the enhanced dispersion interactions developed within the dense monolayer are crucial for bending of the PTCDA admolecules and make the chemisorption state accessible by removing the corresponding energy barrier.

Tersoff−Hamann STM image simulations performed for the optimized densely packed structure revealed a significantly different appearance of the chemisorbed PTCDA molecules in comparison to the physisorbed species. Thus, the observed dramatic contrast change can be assigned to the large distortion of the PTCDA molecule backbone giving rise to breaking of the two-fold symmetry of the chemisorbed state STM contrast. Consequently, instead of the two-lobe feature, which is typical for the physisorbed PTCDA molecules (Figure 6a,b), a uniform single-lobe appearance was recorded for the molecules tightly packed within the monolayer (Figure 6c-e).

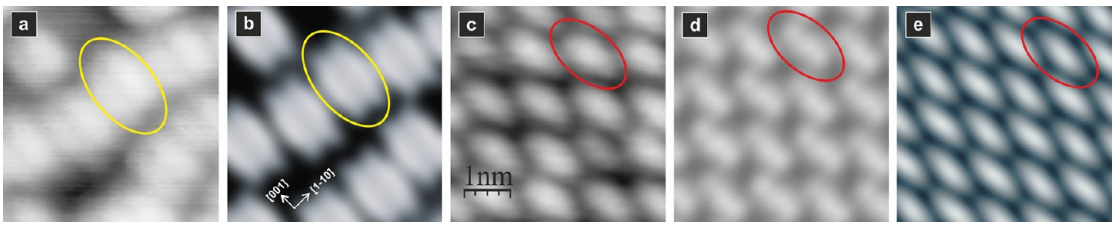

Figure 6. Comparison of the STM contrasts for the physisorbed and chemisorbed PTCDA molecules. Experimental (a) and calculated Tersoff−Hamann (b) images of the physisorbed meandering molecular stripes (yellow ellipses indicate single molecules). Experimental (c) and calculated Tersoff−Hamann (d) and Bardeen (e) images of the chemisorbed (6 × 2) superstructure (red ellipses indicate single molecules). Images (a−d) were simulated with the bias voltage of +2.0 V and the tunneling current of 2 pA; image (e) was simulated in the constant height mode at bias voltage of +2.0 V.

The supramolecular structure obtained at the monolayer coverage can be described as a well-known PTCDA herringbone phase,[14] which is additionally distorted due to significant non-uniform rotation of the molecules and unidirectional arching of all molecules over the surface oxygen rows, leading to the (6 × 2) symmetry of the superstructure unit cell. Despite the two distinct orientations of the molecules within the monolayer of the herringbone structure, such collective bulging of the central part of each molecule leads to an unexpected almost brick-wall *c*(6 × 2) appearance in the STM images seen in Figure 6c-e.

The herringbone structure is typically formed by PTCDA molecules deposited on well-defined substrates with a "flat" surface−molecule interaction potential that is significantly weaker than the intermolecular ordering forces and therefore does not provide any specific adsorption sites. On such substrates, the supramolecular structures can be ordered readily by intermolecular forces, as for example, on the Au(111) surface.[49] In the present study on the PTCDA/TiO_2(110) system, the supramolecular ordering is strongly affected by the pronounced anisotropy of the surface structure with the crucial role played by the protruding oxygen rows. The latter create a ripple-like surface potential that in conjunction with the intermolecular dispersion forces have a significant effect on the ordering and configuration of the PTCDA molecules. Consequently, the structure of the full monolayer is very similar to the herringbone pattern, comprising considerably distorted PTCDA molecules that adopt their own geometry to the (110) surface landscape by arching over the terminal oxygen rows. Such configuration with hydrogen atoms directed toward the surface is stabilized by collective action of intermolecular dispersion forces and establishment of chemical bonds with surface titanium atoms. Interestingly, for the alternative configuration with the hydrogen atoms directed out of the surface a Tersoff−Hamann based simulation gives rise to significantly different STM pattern (see Figure S6 in Supporting Information) with molecule images rotated with respect to the direction pointed by substrate surface oxygen rows. Noting a rather crude approximation of the Tersoff−Hamann approach, we supplemented the simulations for the most stable configuration by the much more advanced Bardeen approach in order to minimize the uncertainties associated with STM image simulations. Indeed, this more accurate method gives rise to even better agreement with the experimental pictures (Figure 6e).

In order to factorize the stabilization energy (2.79 eV) of a PTCDA admolecule within the monolayer into the admolecule-surface and the intermolecular contributions, we performed calculations for the isolated PTCDA admolecule in a frozen geometry adopted from the monolayer coverage. The calculated PTCDA−surface interaction energy was equal to 1.75 eV, allowing for extraction of the intermolecular stabilization energy for the molecule within the densely packed layer, which reaches 1.04 eV. Hence, overcoming the energetic barrier (0.52 eV) of the pronounced distortion of the chemisorbed PTCDA species can be explained by the enhancement of the intermolecular dispersion forces caused by an increased number of the adjacent molecules once the dense monolayer is being formed. It is thus clear that the intermolecular contribution plays a key role in the bending of the molecule backbone and the formation of chemical bonds, which due to steric constraints imposed by the protruding oxygen rows cannot be achieved for a single PTCDA molecule. Yet, the structural relaxation of the single PTCDA molecule with the bent geometry taken from the monolayer structure is only moderate and, accidentally, its total binding energy (E_{ads} = 1.80 eV) is very similar to that obtained for the physisorbed PTCDA (1.76 eV). However, the lack of the chemisorbed states in STM images at the low coverage limit can be clarified not only by the already discussed bending energy barrier but also by unfavorable adsorption thermodynamics. Indeed, the free enthalpy of the adsorption, ΔG_{ads}, showed that at the temperature above 50 K only the physisorbed state of the

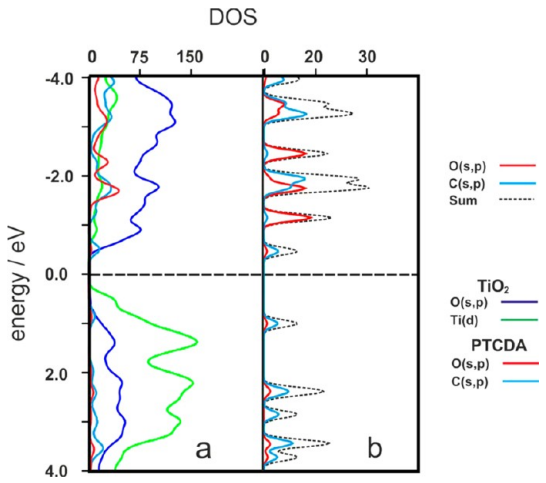

Figure 7. Density of states (DOS) diagrams for the PTCDA monolayer on rutile (110) surface (a) and an isolated physisorbed PTCDA molecule (b).

PTCDA admolecules is clearly preferred once the entropic term is taken into account (see Supporting Information Figure S3).

To illustrate the importance of dispersion forces in monolayer self-assembly, we repeated modeling within the pure DFT method without inclusion of the dispersion interactions. The results showed that PTCDA molecules remain essentially flat upon adsorption and their stacking due to the space limitation gives rise to a roof-tiles structure (see Supporting Information, Figure S5) in which the protruding admolecules are not evenly distributed on the surface. This result clearly contradicts the STM and LEED experiments. In such a geometry, PTCDA stabilization energy falls to mere 0.24 eV in dramatic contrast to PTCDA stabilization of 2.79 eV in a monolayer with dispersion interactions incorporated.

Influence of the Adsorption Mode on the Electronic Structure of the PTCDA/TiO_2 Assembly. The observed transformation from the flat physisorbed into the bent chemisorbed state can be used to control the electronic and optoelectronic properties of the organic dye sensitizers, which strongly depend on the molecular structure of the adspecies. It also demonstrates feasibility of controlled structural transitions in the supramolecular surface assemblies and the resultant alteration in the functional behavior of the oxide photonic devices with variation of the surface coverage.

To study the influence of the PTCDA adsorption mode on photosensitization properties of the PTCDA/TiO_2 system, we discussed the energy level alignment at the PTCDA/TiO_2(110) interface by calculating density of states (DOS) diagrams. In Figure 7, the DOS for the PTCDA/TiO_2(110) monolayer (left panel) and single physisorbed PTCDA molecule (right panel) are shown. The pattern for the single molecule consists of narrow bands, which originate from strongly localized electrons on the s and p orbitals of the carbon (mainly in the sp^2 hybridization) and oxygen PTCDA atoms. The highest occupied states (originating from HOMO) lie 1.5 eV below the lowest unoccupied states (originating from LUMO). The overall DOS structure is very close to that of a molecule in the gas phase, indicating only weak electronic coupling between rutile and PTCDA, which is unfavorable for photonic applications.

The left panel in Figure 7 shows the DOS of the PTCDA monolayer chemisorbed on the (110) rutile surface. Due to the bending of PTCDA molecules, the DOS bands are clearly broadened. Furthermore, when compared to the DOS of the physisorbed molecule, the HOMO band remains practically unshifted while the LUMO band is lowered by 0.02 eV. The C(s,p) states emerge above the top of the valence band, indicating the electronic promotion of TiO_2. The bottom of the conduction band of TiO_2 remains almost intact, whereas the LUMO band is located directly above the bottom of the conduction band in accordance with recent experimental studies.[50] Such relative energy alignment and strong electronic coupling between the chemisorbed PTCDA adspecies and the TiO_2 substrate due to covalent C—O—Ti bonds are favorable for electron injection from the photoexcited PTCDA dye into the sensitized titanium oxide and for interfacial charge delocalization as discussed by Cao *et al.*[50]

CONCLUSIONS

We have demonstrated experimentally and rationalized by modeling the ability of large, planar organic molecules, exemplified by PTCDA, to arch over the protruding oxygen rows on the TiO_2(110) surface by collective action of the intermolecular dispersive forces, which allows for strong electronic coupling between the dye adspecies and the TiO_2 substrate. This effect is of particular importance on highly anisotropic surfaces, where the dispersive forces can dominate the intrinsically complex molecule—substrate interaction landscape. High-resolution STM and LEED results complemented by DFT-D calculations have demonstrated remarkable transition in the mode of PTCDA adsorption as a function of coverage, which is directly controlled by the strength of the interfacial and the intermolecular dispersion interactions. At submonolayer coverage, the interfacial dispersion forces play a dominant role in the adsorption of single flat-lying PTCDA molecules in a nearly intact state, whereas the intermolecular dispersion interactions are decisive in the self-organization of PTCDA at higher submonolayer coverages into meandering molecular stripes. When a monolayer is formed, molecule—substrate and intermolecular dispersion forces lead collectively to the formation of a commensurate

dense structure, built of bent chemisorbed species. The resultant alignment of the energy levels and strong electronic coupling at the PTCDA/TiO_2 interface, due to formation of covalent C–O–Ti bonds, are advantageous for potential dye sensitization applications.

METHODS

Experimental Details. The experiments were carried out in an ultrahigh vacuum (UHV) system containing preparation, surface analysis, and radial distribution chambers. The STM measurements were performed with an Omicron variable-temperature scanning probe microscope (VT STM/AFM). The base pressure was in the low 10^{-10} mbar range. The preparation chamber was supplied with a noble gas ion gun, effusion cells, an infrared pyrometer, and a quartz microbalance thickness monitor. The surface quality was monitored with a low-energy electron diffraction (LEED) setup. The TiO_2(110) wafers (MaTecK GmbH) were mounted on sample holders with a silicon wafer underneath acting as a resistive heater. The samples were first annealed for 6 h at 800 K, and subsequently, the cycles of 1 keV Ar^+ sputtering for 15 min and annealing at 960 K for 15 min were repeated until a clean, well-defined surface was obtained, as checked by LEED and STM measurements. The annealing temperature was controlled by the infrared pyrometer. The experimental procedure was adjusted to keep the sample as clean as possible, as the contamination could affect seriously the growth of molecular structures on metal oxides. The PTCDA molecules were evaporated at about 580 K from a Knudsen cell on the TiO_2(110) surface kept at room or elevated temperature. For molecule deposition, the sample was heated by a resistive heater and the temperature was monitored by type K thermocouple. Prior to the evaporation procedure, PTCDA powder (Fluka) was outgassed for several hours in vacuum at the temperature slightly below the sublimation point. The STM imaging was carried out at reduced temperature of around 90 K (flow cryostat, liquid nitrogen) in a constant current mode at positive bias voltages (empty state imaging) with etched tungsten tips used as probes. For image processing and STM data analysis, WSxM software[51] was used.

Calculation Scheme. For all calculations, we chose the first principles DFT theory implemented in the Vienna Ab initio Simulations Package (VASP)[52] based on Mermin's finite temperature DFT.[53] We employed the projector augmented plane wave (PAW) method[54,55] for describing electron–ion interactions together with PW91 GGA exchange-correlation functional as parametrized by Perdew *et al.* based on the fact that the GGA functionals can produce reliable results in describing electronic structure of oxide systems like titania.[56–58]

Presented results were obtained for the standard Monkhorst-Pack grid[59] ($3 \times 3 \times 2$ sampling mesh for bulk calculations and $2 \times 2 \times 1$ for slab calculations) with the cutoff energy of 380 eV and the Methfessel–Paxton smearing[60] with σ parameter set to 0.1 eV. For solving the Kohn–Sham equations, the self-consistent field (SCF) convergence criterion was set to be an energy change not larger than 10^{-5} eV between two successive iterations.

Surface geometries were constructed by cleaving the crystal along the (110) plane. The supercell models with stoichiometry of $Ti_{72}O_{144}$ were built to describe both adsorption of an isolated PTCDA molecule and monolayer structure (for periodic model details, see Figure S4 and Tables S3 and S4 in the Supporting Information). The size of the surface model was adequate to accommodate two PTCDA molecules in the supercell. Geometry optimization was performed until the changes in the forces acting on the ions were smaller than 0.001 eV/Å per atom. The molecular dynamics (MD) calculations of monolayer were carried with the following settings: Nose-Hoover chain (2) thermostat, time step 10 fs, and the Nose coupling parameter of 2.0. The integration was performed for the total of 1000 steps.

With the optimized geometries of the PTCDA molecules, the resultant STM image simulations were performed as topographs of constant local density of states within the Tersoff–Hamann theory.[47] The images were simulated in the constant current (I = 2 pA) mode applied in the STM experiments and the local density of states as constructed from electronic states in an energy window between 0 and 2 eV above the Fermi level (*i.e.*, empty states). Taking into account the complexity of the monolayer, we have verified the Tersoff–Hamann simulations with much more advanced Bardeen approach[48] as implemented in the bSKAN code.[61,62] The tunneling current was evaluated in a constant height mode as a convolution of the substrate and tip densities of states. In the simulations, bias voltage (from 0.75 to 2.0 V), tip–surface distance (from 1 to 3 Å), and the tip geometries (square pyramid, square pyramid with single W atom, and square pyramid terminated with 2×2 ensemble of W atoms) were tested.

In the computation procedure, the dispersion semi-empirical terms parametrized by Grimme and applied successfully for modeling interactions between hydrocarbons and metal oxides[34,35] were added to the quantum-mechanical energies and gradients (DFT-D method).

Conflict of Interest: The authors declare no competing financial interest.

Acknowledgment. The research was supported by the Polish Ministry of Science and Higher Education under Grant No. 1802/B/H03/2010/38. S.G. acknowledges financial support received from the Foundation for Polish Science within START program (2010 and 2011). A.T. gratefully acknowledges the Natural Sciences and Engineering Research Council of Canada for financial support as a Vanier Canada Graduate Scholar. F.Z. acknowledges the financial support from the Faculty of Chemistry for young scientists. This research was carried out with the equipment purchased thanks to the financial support of the European Regional Development Fund in the framework of the Polish Innovation Economy Operational Program (Contract No. POIG.02.01.00-12-023/08).

Supporting Information Available: Additional experimental and calculations details. This material is available free of charge *via* the Internet at http://pubs.acs.org.

REFERENCES AND NOTES

1. Gao, W.; Dickinson, L.; Grozinger, C.; Morin, F. G.; Reven, L. Order–Disorder Transitions in Self-Assembled Monolayers: A ^{13}C Solid-State NMR Study. *Langmuir* **1997**, *13*, 115–118.
2. Grirrane, A.; Corma, A.; Garcia, H. Gold-Catalyzed Synthesis of Aromatic Azo Compounds from Anilines and Nitroaromatics. *Science* **2008**, *322*, 1661–1664.
3. Ruiz, A. M.; Cornet, A.; Shimanoe, K.; Morante, J. R.; Yamazoe, N. Effects of Various Metal Additives on the Gas Sensing Performances of TiO_2 Nanocrystals Obtained from Hydrothermal Treatments. *Sens. Actuators, B* **2005**, *108*, 34–40.
4. Paulios, I.; Spathis, P.; Grigoriadou, A.; Delidou, K.; Tsoumparis, P. Protection of Marbles Against Corrosion and Microbial Corrosion with TiO_2 Coatings. *J. Environ. Sci. Health, Part A* **1999**, *34*, 1455–1471.
5. Hernandez-Alonso, M. D.; Tejedor, I.; Coronado, J. M.; Soria, J.; Anderson, M. A. Sol–Gel Preparation of TiO_2–ZrO_2 Thin Films Supported on Glass Rings: Influence of Phase Composition on Photocatalytic Activity. *Thin Solid Films* **2006**, *502*, 125–131.
6. Lamaka, S. V.; Zheludkevich, M. L.; Yasakau, K. A.; Serra, R; Poznyak, S. K.; Ferreira, M. G. S. Nanoporous Titania Interlayer as Reservoir of Corrosion Inhibitors for Coatings with Self-Healing Ability. *Prog. Org. Coat.* **2007**, *58*, 127–135.
7. Li, B.; Zhao, J.; Onda, K.; Jordan, O. K. D.; Yang, J.; Petek, H. Ultrafast Interfacial Proton-Coupled Electron Transfer. *Science* **2006**, *311*, 1436–1440.

8. Diebold, U. The Surface Science of Titanium Dioxide. *Surf. Sci. Rep.* **2003**, *48*, 53–229.
9. Palmgren, P.; Yu, S.; Hennies, F.; Nilson, K.; Akemark, B.; Goethelid, M. Changing Adsorption Mode of FePc on TiO_2(110) by Surface Modification with Bipyridine. *J. Chem. Phys.* **2008**, *129*, 074707.
10. Chi, L. P.; Lindsay, R.; Thornton, G. Chemical Reactions on Rutile TiO_2(110). *Chem. Soc. Rev.* **2008**, *37*, 2328–2353.
11. Godlewski, S.; Tekiel, A.; Prauzner-Bechcicki, J. S.; Budzioch, J.; Gourdon, A.; Szymonski, M. Adsorption of Organic Molecules on the TiO_2(011) Surface: STM Study. *J. Chem. Phys.* **2011**, *134*, 224701.
12. Rohlfing, M.; Temirov, R.; Tautz, F. S. Adsorption Structure and Scanning Tunneling Data of a Prototype Organic−Inorganic Interface: PTCDA on Ag(111). *Phys. Rev. B* **2007**, *76*, 115421.
13. Romaner, L.; Nabok, D.; Puschnig, P.; Zojer, E.; Ambrosch-Draxl, C. Theoretical Study of PTCDA Adsorbed on the Coinage Metal Surfaces, Ag(111), Au(111), and Cu(111). *New J. Phys.* **2009**, *11*, 053010.
14. Tautz, F. S. Structure and Bonding of Large Aromatic Molecules on Noble Metal Surfaces: The Example of PTCDA. *Prog. Surf. Sci.* **2007**, *82*, 479–520.
15. Temirov, R.; Soubatch, S.; Luican, A.; Tautz, F. S. Free-Electron-like Dispersion in an Organic Monolayer Film on a Metal Substrate. *Nature* **2006**, *444*, 350–353.
16. Soubiron, T.; Vaurette, F.; Nys, J. P.; Grandidier, B.; Wallart, X.; Stiévenard, D. Molecular Interactions of PTCDA on Si(100). *Surf. Sci.* **2005**, *581*, 178–188.
17. Zahn, D. R. T.; Gavrila, G. N.; Salvan, G. Electronic and Vibrational Spectroscopies Applied to Organic/Inorganic interfaces. *Chem. Rev.* **2007**, *107*, 1161–1232.
18. Burke, S. A.; Ji, W.; Mativetsky, J. M.; Topple, J. M.; Fostner, S.; Gao, H.-J.; Guo, H.; Grütter, P. Strain Induced Dewetting of a Molecular System: Bimodal Growth of PTCDA on NaCl. *Phys. Rev. Lett.* **2008**, *100*, 186104.
19. Kunstmann, T.; Schlarb, A.; Fendrich, M.; Wagner, T.; Möller, R.; Hörmann, R. Dynamic Force Microscopy Study of 3,4,9,10-Perylenetetracarboxylic Dianhydride on KBr(001). *Phys. Rev. B* **2005**, *71*, 121403.
20. Tkatchenko, A.; Romaner, L.; Hofmann, O. T.; Zojer, E.; Ambrosch-Draxl, C.; Scheffler, M. van der Waals Interactions between Organic Adsorbates and at Organic/Inorganic Interfaces. *MRS Bull.* **2010**, *35*, 435–442.
21. Classen, T.; Lingenfelder, M.; Wang, Y.; Chopra, R.; Virojanadara, C.; Starke, U.; Costantini, G.; Fratesi, G.; Fabris, S.; De Gironcoli, S.; Baroni, S.; Haq, S.; Raval, R.; Kern, K. Hydrogen and Coordination Bonding Supramolecular Structures of Trimesic Acid on Cu(110). *J. Phys. Chem. A* **2007**, *111*, 12589–12603.
22. Duhm, S.; Heimel, G.; Salzmann, I.; Glowatzki, H.; Johnson, R. L.; Vollmer, A.; Rabe, J. P.; Koch, N. Orientation-Dependent Ionization Energies and Interface Dipoles in Ordered Molecular Assemblies. *Nat. Mater.* **2008**, *7*, 326–332.
23. Lu, Y.; Quardokus, R.; Lent, C. S.; Justaud, F.; Lapinte, C. S.; Kandel, A. Charge Localization in Isolated Mixed-Valence Complexes: An STM and Theoretical Study. *J. Am. Chem. Soc.* **2010**, *132*, 13519–13524.
24. Márquez, A. M.; Plata, J. J.; Sanz, J. F. Role of Coverage and Surface Oxidation Degree in the Adsorption of Acetone on TiO_2 (110). A Density Functional Study. *J. Phys. Chem. C* **2009**, *113*, 19973–19980.
25. Ohmann, R.; Levita, G.; Vitali, L.; De Vita, A.; Kern, K. Influence of Subsurface Layers on the Adsorption of Large Organic Molecules on Close-Packed Metal Surfaces. *ACS Nano* **2011**, *5*, 1360–1365.
26. Pastore, M.; De Angelis, F. Aggregation of Organic Dyes on TiO_2 in Dye-Sensitized Solar Cells Models: An *Ab Initio* Investigation. *ACS Nano* **2010**, *4*, 556–562.
27. Walsh, M. A.; Walter, S. R.; Bevan, K. H.; Geiger, F. M.; Hersam, M. C. Phenylacetylene One-Dimensional Nanostructures on the Si(100)-2×1:H Surface. *J. Am. Chem. Soc.* **2010**, *132*, 3013–3019.
28. Weiss, C.; Wagner, C.; Kleimann, C.; Rohlfing, M.; Tautz, F. S.; Temirov, R. Imaging Pauli Repulsion in Scanning Tunneling Microscopy. *Phys. Rev. Lett.* **2010**, *105*, 086103.
29. Zasada, F.; Piskorz, W.; Godlewski, S.; Prauzner-Bechcicki, J. S.; Tekiel, A.; Budzioch, J.; Cyganik, P.; Szymonski, M.; Sojka, Z. Chemical Functionalization of the TiO_2(110)-(1×1) Surface by Deposition of Terephthalic Acid Molecules. A Density Functional Theory and Scanning Tunneling Microscopy Study. *J. Phys. Chem. C* **2011**, *115*, 4134–4144.
30. Martsinovich, N.; Jones, D. R.; Troisi, A. Electronic Structure of TiO_2 Surfaces and Effect of Molecular Adsorbates Using Different DFT Implementations. *J. Phys. Chem. C* **2010**, *114*, 22659–22670.
31. Nilsing, M.; Persson, P.; Lunell, S.; Ojamäe, L. Dye-Sensitization of the TiO_2 Rutile (110) Surface by Perylene Dyes: Quantum-Chemical Periodic B3LYP Computations. *J. Phys. Chem. C* **2007**, *111*, 12116–12123.
32. Atodiresei, N.; Caciuc, V.; Lazic, P.; Blügel, S. Chemical *versus* van der Waals Interaction: The Role of the Heteroatom in the Flat Absorption of Aromatic Molecules C_6H_6, C_5NH_5, and $C_4N_2H_4$ on the Cu(110) Surface. *Phys. Rev. Lett.* **2009**, *102*, 136809.
33. Mercurio, G.; McNellis, E. R.; Martin, I.; Hagen, S.; Leyssner, F.; Soubatch, S.; Meyer, J.; Wolf, M.; Tegeder, P.; Tautz, F. S.; Reuter, K. Structure and Energetics of Azobenzene on Ag(111): Benchmarking Semiempirical Dispersion Correction Approaches. *Phys. Rev. Lett.* **2010**, *104*, 036102.
34. Grimme, S. Accurate Description of van der Waals Complexes by Density Functional Theory Including Empirical Corrections. *J. Comput. Chem.* **2004**, *25*, 1463–1473.
35. Grimme, S. Semiempirical GGA-Type Density Functional Constructed with a Long-Range Dispersion Correction. *J. Comput. Chem.* **2006**, *27*, 1787–1799.
36. Wu, Q.; Yang, W. Empirical Correction to Density Functional Theory for van der Waals Interactions. *J. Chem. Phys.* **2002**, *116*, 515–524.
37. Jurecka, P.; Cerny, J.; Hobza, P.; Salahub, D. Density Functional Theory Augmented with an Empirical Dispersion Term. Interaction Energies and Geometries of 80 Noncovalent Complexes Compared with *Ab-Initio* Quantum Mechanics Calculations. *J. Comput. Chem.* **2007**, *28*, 555–569.
38. Atodiresei, N.; Caciuc, V.; Franke, J.-H.; Blugel, S. Role of the van der Waals Interactions on the Bonding Mechanism of Pyridine on Cu(110) and Ag(110) Surface: First-Principles Study. *Phys. Rev. B* **2008**, *78*, 045411.
39. Tkatchenko, A.; Scheffler, M. Accurate Molecular van der Waals Interactions from Ground-State Electron Density and Free-Atom Reference Data. *Phys. Rev. Lett.* **2009**, *102*, 073005.
40. McNellis, E. R.; Meyer, J.; Baghi, A. D.; Reuter, K. Stabilizing a Molecular Switch at Solid Surfaces: A Density Functional Theory Study of Azobenzene on Cu(111), Ag(111), and Au(111). *Phys. Rev. B* **2009**, *80*, 035414.
41. McNellis, E. R.; Meyer, J.; Reuter, K. Azobenzene at Coinage Metal Surfaces: Role of Dispersive van der Waals Interactions. *Phys. Rev. B* **2009**, *80*, 205414.
42. Shi, X.; Zhang, R. Q.; Minot, C.; Hermann, K.; Van Hove, M. A.; Wang, W.; Lin, N. Complex Molecules on a Flat Metal Surface: Large Distortions Induced by Chemisorption Can Make Physisorption Energetically More Favorable. *J. Phys. Chem. Lett.* **2010**, *1*, 2974–2979.
43. Nguyen, M.-T.; Pignedoli, C. A.; Treier, M.; Fasel, R.; Passerone, D. The Role of van der Waals Interactions in Surface-Supported Supramolecular Networks. *Phys. Chem. Chem. Phys.* **2010**, *12*, 992–999.
44. Martinez-Casado, R.; Mallia, G.; Usvyat, D.; Maschio, L.; Casassa, S.; Schütz, M.; Harrison, N. M. Periodic Quantum Mechanical Simulation of the He−MgO(100) Interaction Potential. *J. Chem. Phys.* **2011**, *134*, 014706.
45. Sorescu, D. C.; Lee, J.; Al-Saidi, W. A.; Jordan, K. D. CO_2 Adsorption on TiO_2(110) Rutile: Insight from Dispersion-Corrected Density Functional Theory Calculations and Scanning Tunneling Microscopy Experiments. *J. Chem. Phys.* **2011**, *134*, 104707.

46. Zhang, Z.; Rousseau, R.; Gong, J.; Kay, B. D.; Dohnalek, Z. Imaging Hindered Rotations of Alkoxy Species on TiO_2-(110). *J. Am. Chem. Soc.* **2009**, *131*, 17926–17932.
47. Tersoff, J.; Hamann, D. R. Theory of the Scanning Tunneling Microscope. *Phys. Rev. B* **1985**, *31*, 805.
48. Bardeen, J. Tunnelling from a Many-Particle Point of View. *Phys. Rev. Lett.* **1961**, *6*, 57.
49. Hauschild, A.; Karki, K.; Cowie, B. C. C.; Rohlfing, M.; Tautz, F. S.; Sokolowski, M. Molecular Distortions and Chemical Bonding of a Large π-Conjugated Molecule on a Metal Surface. *Phys. Rev. Lett.* **2005**, *94*, 036106.
50. Cao, L.; Wang, Y.; Zhong, J.; Han, Y.; Zhang, W.; Yu, X.; Xu, F.; Qi, D.-C.; Wee, A. T. S. Electronic Structure, Chemical Interactions and Molecular Orientations of 3,4,9,10-Perylene-tetracaboxylic-dianhydride on TiO_2(110). *J. Phys. Chem. C* **2011**, *115*, 24880–24887.
51. Horcas, I.; Fernandez, R.; Gomez-Rodriguez, J. M.; Colchero, J.; Gomez-Herrero, J.; Baro, A. M. WSXM: A Software for Scanning Probe Microscopy and a Tool for Nanotechnology. *Rev. Sci. Instrum.* **2007**, *78*, 013705.
52. Hafner, J. *Ab-Initio* Simulations of Materials Using VASP: Density-Functional Theory and Beyond. *J. Comput. Chem.* **2008**, *29*, 2044–2078.
53. Mermin, N. D. Thermal Properties of the Inhomogeneous Electron Gas. *Phys. Rev.* **1965**, *137*, A1141.
54. Blöchl, P. E. Projector Augmented-Wave Method. *Phys. Rev. B* **1994**, *50*, 17953.
55. Kresse, G.; Joubert, J. From Ultrasoft Pseudopotentials to the Projector Augmented-Wave Method. *Phys. Rev. B* **1999**, *59*, 1758.
56. Di Valentin, C. Scanning Tunneling Microscopy Image Simulation of the Rutile (110) TiO_2 Surface with Hybrid Functionals and the Localized Basis Set Approach. *J. Chem. Phys.* **2007**, *127*, 154705-1.
57. Labat, F.; Baranek, P.; Domain, C.; Minot, C.; Adamo, C. Density Functional Theory Analysis of the Structural and Electronic Properties of TiO_2 Rutile and Anatase Polytypes: Performances of Different Exchange-Correlation Functionals. *J. Chem. Phys.* **2007**, *126*, 154703-1.
58. Hammer, B.; Wendt, S.; Besenbacher, F. Water Adsorption on TiO_2. *Top. Catal.* **2010**, *53*, 423–430.
59. Monkhorst, H. J.; Pack, J. D. Special Points for Brillouin-Zone Integrations. *Phys. Rev. B* **1976**, *13*, 5188.
60. Methfessel, M.; Paxton, A. T. High-Precision Sampling for Brillouin-Zone Integration in Metals. *Phys. Rev. B* **1989**, *40*, 3616.
61. Hofer, W. A.; Foster, A. S.; Schluger, A. L. Theories of Scanning Probe Microscopes at the Atomic Scale. *Rev. Mod. Phys.* **2003**, *75*, 1287–1331.
62. Hofer, W. A.; Redinger, J. Scanning Tunneling Microscopy of Binary Alloys: First Principles Calculation of the Current for PtX (100) Surfaces. *Surf. Sci.* **2000**, *447*, 51–61.